Final Report: Exploring Policies For Disease Identification In Chest X-rays
https://www.youtube.com/watch?v=l7Yz6lREtdg

Martin Saint-Jalmes[1], **Reynaldo Pena**[1]
[1]**Georgia Institute of Technology, Atlanta, GA, USA**

Abstract

This project aims to analyze radiographic lung images from the CheXpert Stanford hospital dataset to determine whether they have a lung disease and, if so, which disease they have. It relies on convolutional neural networks to learn from images, as well as big data tools to preprocess information. We explore several means to attempt to improve model AUC score, including data augmentation techniques and varying policies to handle uncertain and implicit data. The goal is to provide a supplement to health workers to better diagnose diseases. We provide our code[2] *and results.*

Introduction

Radiographic image disease classification is an important task in order to aid health workers better diagnose diseases and to save time doing so. The goal of this project is to create a lung radiographic image disease detection model to help doctors improve their disease diagnoses accuracy, especially when there is no clear consensus on the diagnosis. This is important because as many as five percent of U.S. adults receive incorrect diagnosis annually (Such et al. (2017)), and early correct diagnosis can save peoples' lives. Disease misdiagnosis has a huge cost for patients each year, ranging from misplaced and delayed treatments to death. A study conducted by the John Hopkins School of Medicine estimated that up to 80,000 deaths occur each year in the U.S. due to incorrect diagnoses (Newman-Toker et al. (2019)). Thus, this paper attempts to provide radiographers with another tool to improve correct lung disease diagnoses, intended to supplement their own diagnoses with advanced machine learning techniques. Improving the accuracy of the model means increasing the correct disease diagnoses rate, thus saving patients' lives. We use lung radiographic images from the Stanford Chexpert Dataset in RGB format, and then train convolutional neural network models to analyze these images. Our training data has fourteen response variables, and each variable has four possible outcomes: Positive (has disease), Uncertain, Negative, Implicit Negative (no *mention* of disease). Uncertain refers to cases where the doctor was not certain about the diagnosis. The main goal of this project is to find ways to best deal with the uncertain and implicit negative classifications in order to improve diagnoses, since this is where most improvement can be done. Our test set only presents Positive & Negative outcomes, but the distribution may be unbalanced so we use AUC as the means to evaluate our models.

Related Work

(Irvin et al. (2019)) describe the motivation for the release of the CheXpert dataset, one of the largest datasets of chest x-rays. Along with the dataset, the paper describes the labeling tool that was used to create the ground truth labels for this dataset (from freetext reports), an evaluation of the quality of labeling relying on expert appreciation (by several radiologists), and a baseline model for the task of predicting 14 diseases using uncertainty labels. (Pham et al. (2019)) present the state-of-the-art model that their team used to predict the 14 lung diseases and observations from the CheXpert dataset. Their model makes use of hierarchies, based on the interdependances between the diseases. The best AUC performance is achieved with a custom policy for uncertainty labels (label smoothing regularization) and an ensemble of CNNs. (Johnson et al. (2019)) release MIMIC-CXR-JPG, an alternative dataset (bigger than CheXpert), making MIMIC-CXR more accessible (in image JPGs, rather than DICOM format) to non-medical researchers. The labelling of the images from freetext reports was both performed by NegBio and the CheXpert labeling tool, and evaluated. The paper from (Ranjan et al. (2018)) describe the reasoning behind an alternative representation in the task of predicting diseases for the ChestX-ray14 dataset. They obtain better performance than other models at the time by using auto-encoders as preprocessing to retain information from the high-dimensional X-Ray images rather than downsampling the raw images as input for ImageNet (224x224). (Ge et al. (2018)) justify the use of bilinear pooling and a custom loss function (multi-label learning loss) to jointly learn a model that may take into account interactions

[2] https://github.gatech.edu/msaintjalmes3/CheXpert (shared with Ming Liu and Su Young Park)

between lung diseases on the ChestX-ray14 dataset. Their results show that such a method may improve overall AUC, and boost smaller architectures' performances. (Guan et al. (2018)) tackle the classification task from a different perspective than most papers, relying on spatial information in X-Rays to use an attention-learning technique. At the time of publication, their technique outperformed the state-of-the-art on the ChestX-ray14 dataset. The paper (Rubin et al. (2018)) offers some insight on using the relation between frontal and lateral X-Ray when training CNNs. Using their DualNet architecture, they were able to (most of the time) get better AUCs on the ChestX-ray14 dataset than if the frontal and lateral images had been used separately.

Approach & Implementation

Dataset

The dataset we used in this study is the CheXpert dataset from (Irvin et al. (2019)). The data consists of 224,316 chest radiographs of 65,240 patients. Some patients have multiple radiographs corresponding to side and front chest images. The chest radiographs were gathered from the Stanford hospital between 2002-2017. The images were labeled automatically from freetext radiology reports with a tool identifying mentions of 14 different diseases with a label of Positive, Negative, or Uncertain for each disease. Figure 1 shows the distribution of labels within CheXpert (we note they don't add to 100 as one patient may have multiple diseases). Finally, it is important to note that, as labels were generated (as opposed to human-picked), one can make a slight distinction between "explicit" and "implicit" negative labels: a radiology report may clearly state the absence of a certain disease ("explicit" negative), but not explicitly mention that every single of the other 14 diseases is absent. The policy regarding the handling of implicit negative and uncertain labels is a part of our experiment.

Pathology	Positive (%)	Uncertain (%)	Negative (%)
No Finding	16627 (8.86)	0 (0.0)	171014 (91.14)
Enlarged Cardiom.	9020 (4.81)	10148 (5.41)	168473 (89.78)
Cardiomegaly	23002 (12.26)	6597 (3.52)	158042 (84.23)
Lung Lesion	6856 (3.65)	1071 (0.57)	179714 (95.78)
Lung Opacity	92669 (49.39)	4341 (2.31)	90631 (48.3)
Edema	48905 (26.06)	11571 (6.17)	127165 (67.77)
Consolidation	12730 (6.78)	23976 (12.78)	150935 (80.44)
Pneumonia	4576 (2.44)	15658 (8.34)	167407 (89.22)
Atelectasis	29333 (15.63)	29377 (15.66)	128931 (68.71)
Pneumothorax	17313 (9.23)	2663 (1.42)	167665 (89.35)
Pleural Effusion	75696 (40.34)	9419 (5.02)	102526 (54.64)
Pleural Other	2441 (1.3)	1771 (0.94)	183429 (97.76)
Fracture	7270 (3.87)	484 (0.26)	179887 (95.87)
Support Devices	105831 (56.4)	898 (0.48)	80912 (43.12)

Figure 1: Data set label distribution (reproduced from (Irvin et al. (2019)))

There are a few statistical observations we can make on this dataset. The first relates to the obvious class imbalance, and how it is more or less significant across labels. This imbalance is particularly important in the case of "Pleural Other" (97.76% negative), with almost as many uncertain observations than positive ones. Conversely, "Lung Opacity" is rather balanced (48.3% negative), with litte uncertainty. Aside from the per-disease distribution, it is also important to consider how these are represented per-patient. We looked into statisics over multiple studies and found that the mean number of medical observations (except "No Finding") per patient is between 2.858 and 3.731 (whether the uncertain labels are classified as negative or positive). Furthermore, out of the 64540 patients of the training set, between 8500 and 12199 only have one disease. Conversely, between 74 and 409 extreme cases can be found having more than 10 medical observations. We studied the Pearson correlations between the diseases in order to find if some pairs are commonly found together. "Pleural Effusion" is often found with other observations. Its correlation is 0.423 with "Lung Opacity", 0.364 with "Edema" and 0.320 with "Support Devices". Other less significant correlations involve the "Edema"/"Cardiomegaly" pair (0.314).

For this work, we used the downsampled version of the CheXpert dataset where images are resized to a height of 320 pixels. This serves practical purposes, with the dataset being lighter (11 gigabytes instead of 439) and faster to process. The CNN architectures and models we considered using here all required input images to be resized to 224 by 224 pixels, so we wouldn't have been able to use the full potential of the original resolution images.

While there exists a way to evaluate a model on the CheXpert test set, we found the procedure somewhat impractical for evaluating our models rapidly. This is why we used the designated validation split as a stand-in test set, and built our own "internal" validation set to allow us to tune our CNN models. The matter of building this "internal" validation set is discussed in the following subsection.

Preprocessing

Our first preprocessing task consists of building an "internal" validation set for rapid evaluation purposes while fine-tuning a CNN model. Doing so allows us to avoid phenomena like overfitting on training data, so that we can pick an optimal model learned on the training set, but that generalizes well on unseen data (here, the "internal" validation set). Of course, such a process only has value if we change the training split so that it does not overlap with the "internal" validation set. In order to do this, we use the file provided in the CheXpert dataset that described the images from the original dataset, and split it into "internal" training and validation sets. This split is performed in a way such that no same patient can have radiographies both in the training and validation sets in order to reduce any potential biases (some diseases may carry over across multiple radiographies for the same patient). Considering the very big number of observations, we leveraged big data tools to execute this split. Using a Docker image [3] containing Hadoop and Spark, we load the description file into Hadoop Distributed File System (HDFS), and leverage Scala's `randomSplit` method to write two new descriptive files (containing the location of the radiographies and the labels' ground truths) for the "internal" training and validation set. Spark allows us to load the file in memory, perform the split in a distributed manner (using Resilient Distributed Datasets), and write the resulting new files in HDFS. In this same step, we can decide on the policy to experiment on. The specifics are mentioned in a further subsection (*Experiment design and policies*), but we use the same tools with Scala and Spark to replace blank values (corresponding to the "implicit" negatives) and "-1" (uncertain label) with certain constants. Likewise, the preprocessing is done in a distributed manner (with 4 workers), which allows us to process this data more efficiently.

Another preprocessing that leverages big data tools involves finding the per-channel mean and standard deviation of images. Normalizing the batch of images using these values generally yields better results. To find these values, we load the set of training images in HDFS, and use BigDL from (Dai et al. (2019)) to compute distributed representations of the pixels of the images. We can then find the mean and standard deviation values per pixels using Map-Reduce operations from Spark in Scala.

Further preprocessing steps are done directly using Pytorch. While this doesn't use big data tools, applying a series of preprocessing transformations with Pytorch dataloaders is an efficient means of performing data augmentation "on the fly", without creating new radiographies on the hard drive. Preprocessing steps such as resizing to 224 by 224 pixel images, and normalizing using the previously found values are applied to all data loaders. Conversely, data augmentation steps are only applied to the "internal" training data, not the "internal" validation, nor the "internal" test (i.e. real validation) sets. These data augmentation steps involve applying horizontal mirroring (diseases may affect both lungs the same way), color jitter, and light random cropping (which may crop out existing text on top of the radiographies) to ensure better model robustness.

Metrics

Considering our problem setting, we use Binary Cross-Entropy (BCE) as our loss function:

$$L_p(q) = -\frac{1}{N}\sum_{i=1}^{N} y_i \log(p(y_i)) + (1-y_i)\log(1-p(y_i)) \tag{1}$$

This is for example what is also used in (Irvin et al. (2019)), (Pham et al. (2019)), (Guan et al. (2018)) and (Rubin et al. (2018)). The advantage of this loss function is that it allows for some great flexibility in experimenting with policies, as it performs a sigmoid activation. In this case, we're not constrained to use only 0 and 1 as values: (Pham et al. (2019)) use LSR to replace uncertain labels by uniformly sampled values that are close to 0 or 1. In this work, we

[3] http://www.sunlab.org/teaching/cse6250/spring2020/env/env-docker-compose.html

initially set uncertain values to 0.66 and implicit negatives to 0.33 without needing to change the loss function. (Irvin et al. (2019)) explore an alternative loss, masked Binary Cross-Entropy, in order to ignore "uncertain" observations when training:

$$L(X, y) = -\sum_{0} \mathbb{1}\{y_0 \neq u\}[y_0 \log p(Y_0 = 1|X) + (1 - y_0) \log p(Y_0 = 0|X)] \tag{2}$$

We didn't explore this option further, as the "U-ignore" policy relying on this loss didn't show promising results in their original paper.

As we are in an unbalanced setting (Figure 1), we use the area under the receiver operating characteristic (AUROC or AUC). For instance, a baseline model always predicting "No" would yield an expected 98.7% accuracy on "Pleural Other", so it would not be a suitable metric. We use AUC both to compare our results to other papers on the same validation set, and to perform an early stopping during our training phase by measuring AUC on our "internal" validation set. At each epoch, the AUC on the "internal" validation set is measured for each of the 14 diseases. We keep the model with the highest average AUC on the 14 diseases to counter the overfitting problem with too many epochs.

As we look into AUC to benchmark our models, we will also be looking into type 1 and type 2 errors, which will provide us more insight on how our models perform. AUC being a single number-metric, it can only provide a summarized view of the classification task.

Type 1 error is the probability of incorrectly rejecting the null hypothesis, and type 2 error is the probability of incorrectly accepting the null hypothesis. Type 1 error depends largely on the alpha value of the experiment: the lower the alpha, the lower the type 1 error. Type 2 error, on the other hand, is defined as 1-power, and power depends on factors such as the size of the experiment and population variance. In the medical field type 1 and type 2 error are important considerations when conducting experiments, such as testing a new drug or treatment. For example, if scientists are trying to test the effectiveness of a new drug, they may set up an experiment where the null hypothesis is the drug having the same effect on sick patients as a placebo. In this context, type 1 error is the probability of incorrectly concluding that the experimental treatment is better than the placebo. This may lead to the use of the experimental treatment to treat the disease when, in fact, it is no better than no treatment at all and may even be worse. On the other hand, type 2 error would mean that the scientists find that the experimental treatment has the same effect as the placebo. Here, there is a risk that the treatment is forgotten as useless, when in fact it could save lives. In this specific case of Chest disease identification, we'll be looking into the erroneous prediction of a disease when it was absent, as well as failing to identify one when it was present.

Experiment design and policies

As mentioned in (Irvin et al. (2019)), the fact that uncertain labels can be twice as numerous as positive labels makes the choice of a policy to deal with these labels an important one. On select diseases, a better policy can improve AUC by up to 5%, which can be critical in terms of model adequacy. In this work, we introduce an additional choice in policy regarding "implicit" negatives, corresponding to blank values in the dataset. While in all likelihood, the absence of mention of a disease in a report could be considered to be a negative label for this disease, we wanted to encode stronger priors on "explicit" negatives than implicit ones. We therefore experimented in settings where an "implicit" negative was assigned a label of 0 (i.e. same policy as in other works), or 0.33 (tending to 0, but not ruling out an omission in written reports). Likewise, we design different policies regarding the processing of uncertain values (e.g. set them to 1, 0 or 0.66).

Our experiments were run with two different types of architectures, corresponding to some of the state-of-the-art architectures for object recognition: DenseNet-161 from (Huang et al. (2017)) and ResNet-152 from (He et al. (2017)). These models were adapted so that the final layer only outputs 14 values instead of 1000, and we introduced a sigmoid function to retain values in the $[0, 1]$ range. In both cases, we ran experiments training from scratch, or finetuning from pretrained weights (learned from the ImageNet classification task), freezing the lower layers of the networks. All models were run with an Adam optimizer using default values $\beta_1 = 0.9, \beta_2 = 0.999$. The learning rate for models trained from scratch was 10^{-3}, but was lowered to 10^{-4} for finetuning the pretrained models.

In total, 24 experiments were run, corresponding to the cartesian product of two possible policies for implicit negatives (I-Zeros and I-0.33), three for uncertain labels (U-Zeros, U-Ones and I-0.66), two possible architectures (ResNet-152 and DenseNet-161) and two choices, whether the models were trained from scratch of finetuned.

While our initial experiments were run for 5 epochs, we observed from learning curves that we did not reach a point at which the model started overfitting. We then ran subsequent experiments for 10 epochs. Due to time constraints, six of the original experiments could not be reproduced for 10 epochs. These pertained to the some of the I-Zeros ("implicit" negative assigned a 0 label) experiments, so we hope that the results from either the original paper from (Irvin et al. (2019)) or the alternative architecture (ResNet/DenseNet) provide a close enough approximation of the improvements we would have observed if the models had been trained for a longer time.

Experimental evaluation

We ran part of our desired experiments on remote servers rented on Google Cloud Platform (GCP), using an NVIDIA T4 GPU with 16GB of VRAM for about twelve hours per model (six hours for 5 epochs). Due to the GPU's memory limits, the batch sizes were constrained to 48 and 64 (respectively for DenseNet-161 and ResNet-152 models) trained from scratch, and 512 for finetuning models.

In Table 1, we present some of the best scoring models out of the 24 experiments described in the previous section.

	ResNet-152				DenseNet-161			
	I-Zeros	I-0.33			I-Zeros			I-0.33
	U-0.66 scratch 5 epochs	U-0.66 scratch 10 epochs	U-0.66 pretrained 10 epochs	U-Ones scratch 10 epochs	U-0.66 pretrained 5 epochs	U-0.66 scratch 5 epochs	U-Zeros scratch 5 epochs	U-0.66 pretrained 10 epochs
No Finding	0.829	0.807	0.821	0.812	**0.834**	0.786	0.794	0.823
Enlarged Cardiomediastinum	0.460	0.830	0.812	**0.838**	0.512	0.334	0.526	0.826
Cardiomegaly	0.730	**0.832**	0.737	0.817	0.733	0.757	0.803	0.747
Lung Opacity	**0.870**	0.851	0.819	0.856	0.823	0.843	0.859	0.828
Lung Lesion	0.004	0.004	0.022	0.000	**0.060**	0.012	0.015	0.009
Edema	0.815	0.799	0.836	0.790	0.815	0.795	0.791	**0.846**
Consolidation	0.792	0.829	0.811	0.796	0.817	0.759	0.752	**0.839**
Pneumonia	0.391	0.444	0.608	0.286	0.580	0.259	0.228	**0.725**
Atelectasis	0.753	**0.793**	0.761	0.650	0.762	0.777	0.735	0.746
Pneumothorax	0.498	0.445	**0.677**	0.452	0.636	0.447	0.477	0.633
Pleural Effusion	0.860	**0.879**	0.798	0.864	0.820	0.858	0.855	0.826
Pleural Other	0.109	0.066	0.231	0.125	0.278	0.078	0.087	**0.332**
Fracture	0.000	0.000	0.000	0.000	0.000	0.000	0.000	0.000
Support Devices	0.741	**0.833**	0.740	0.820	0.721	0.753	0.794	0.724
Overall Mean AUC	0.561	0.601	0.620	0.579	0.599	0.533	0.551	**0.636**
5-observation focus Mean AUC	0.790	**0.826**	0.789	0.783	0.789	0.789	0.787	0.801

Table 1: AUC scores on the validation set (i.e. "internal" test set), and averages (focus is on the 5 in bold-italics).

In Figure 2, we present the learning curves of our best-scoring model, showing that there is little room for improvement by training the model for more epochs.

In Figure 3, we present the confusion matrices for two medical observations, edema and pleural effusion, resulting from the evaluation of our best-scoring model on the validation set (i.e. our "internal" test set).

Confusion matrices are a common tool to understand and visualize the accuracy of classification models by looking at both the predicted and actual classification values. It is a powerful tool because it allows the reader to visualize the model's accuracy for each class. The confusion matrix provides a holistic overview of the model's accuracy, which is especially useful in data sets with imbalanced classes where accuracy may be misleadingly inflated by predicting solely the majority class.

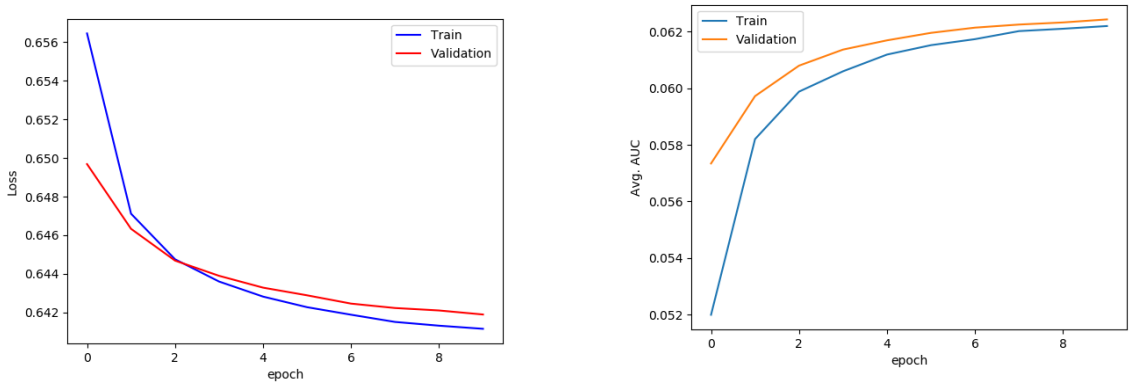

(a) Loss

(b) Overall Mean AUC
(lower bound, ignoring non-0/1 predictions)

Figure 2: Learning curves for the best-scoring model

Looking into confusion matrices allow us to verify our models' type 1 and type 2 errors, as described in the *Metrics* subsection.

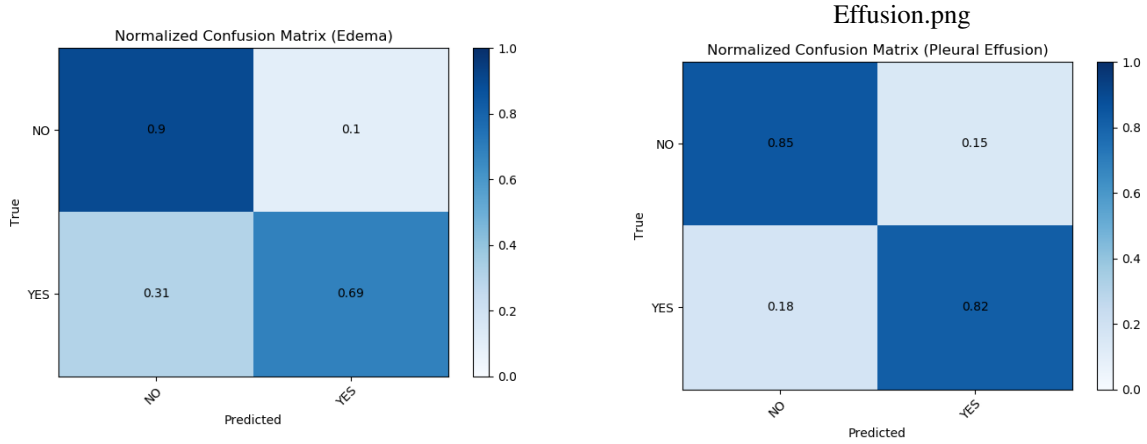

(a) Confusion matrix (Edema)

(b) Confusion matrix (Pleural Effusion)

Figure 3: Some confusion matrices for the best-scoring model

Discussion

The results on the validation set near the baseline (AUC of 0.888) established in (Irvin et al. (2019)) with the *U-Zeros* (implicit=0, uncertain=0) policy on the 5 observations of particular interest (Cardiomegaly, Edema, Consolidation, Atelectasis, Pleural Effusion). Within our 8 best models, we have as many that follow the I-0.33 policy as those that follow the I-Zeros one. The latter corresponds to what is typically done (considering "implicit" and "explicit" negatives the same way). However, within these 8, the two best-scoring models in the 5 observations of particular interest, both implement I-0.33, and the best outperforms I-Zeros models by more than 0.02 AUC. These were also the models that achieved the best results in specific diseases.

The best model's learning curves our training and validation loss and AUC have started to stagnate at the tenth epoch, confirming that training this model longer would not improve performance significantly, and we would start to notice some degree of overfitting. In Figure 3, we notice that we have both reduced to some extent type 1 and 2 errors for Edema and Pleural Effusion. However, the challenge remains to reduce the type 2 error, which is the highest in both cases.

From our best models, we note that half of them correspond to those that were trained early on, and for which we unfortunately couldn't rerun the experiments in time. This is one of the main challenges we faced during this project: as we discovered we should train for longer (10 epochs), this increased significantly the time needed for training (12 hours per model). Given the extent of our experiments (24 combinations), we were unlucky in that some of the best models were among the 6 we couldn't rerun. We acknowledge this result in that the search space of optimization problems is vast and we could have better contrained our experiments (for example, by not looking into learning from scratch or pretrained models).

Finally, despite our best efforts and investigations, we must note the strange results from the "Fracture" class, reproduced over different "internal" training-validation splits. Because our model performs suboptimally on labels that have over 95% negative cases (fracture, pleural other, and lung lesion), we suspect that some improvement can be achieved by reweighting the loss to give more importance in finding true positives of these rarer diseases.

Conclusion & Future work

Correct disease diagnoses is top priority for healthcare professionals. This project sought to create more accurate lung disease diagnosis using radiographic images by applying different preprocessing steps and exploring new policies to handle uncertain and implicit output variables. While our best model was competitive with the original paper's baseline, it fails to reach state of the art performance of the more complex, hierarchical models. However, from our observations, designing policies to handle uncertain and negative implicit labels specifically could outperform traditional preprocessing steps. Future work could focus on the DualNet model (learning separate models for frontal and lateral images with a prior classifier), as it has shown promising results in its original paper. We suggest further investigations in deciding the value for implicit negatives: rather than setting it to 0.33, we could apply label smoothing regularization by sampling the values from a uniform distribution close to 0.

References

1. Such MV, Lohr R, Beckman T, et al. Extent of diagnostic agreement among medical referrals. Journal of Evaluation in Clinical Practice 2017;23:870?4. doi:10.1111/jep.12747
2. Newman-Toker DE, Schaffer AC, Yu-Moe CW, et al. Serious misdiagnosis-related harms in malpractice claims: The "Big Three" - vascular events, infections, and cancers. Diagnosis 2019;6:227?40. doi:10.1515/dx-2019-0019
3. Irvin J, Rajpurkar P, Ko M, et al. CheXpert: A Large Chest Radiograph Dataset with Uncertainty Labels and Expert Comparison. Proceedings of the AAAI Conference on Artificial Intelligence 2019;33:590?7. doi:10.1609/aaai.v33i01.3301590
4. Pham, Hieu H., Le, Tung T., Dat, Tran Q., et al. Interpreting chest X-rays via CNNs that exploit disease dependencies and uncertainty labels. Neurocomputing (preprint) 2019; arXiv:1911.06475v2
5. Johnson, Alistair E. W., et al. MIMIC-CXR, a De-Identified Publicly Available Database of Chest Radiographs with Free-Text Reports. Scientific Data, vol. 6, no. 1, 2019, doi:10.1038/s41597-019-0322-0.
6. Ranjan, Ekagra, et al. Jointly Learning Convolutional Representations to Compress Radiological Images and Classify Thoracic Diseases in the Compressed Domain Proceedings of the Twelfth Indian Conference on Computer Vision, Graphics and Image Processing, 2018, doi:10.1145/3293353.3293408
7. Ge, Zongyuan, et al. Chest X-rays Classication a Multi-Label and Fine-Grained Problem, 2018, arXiv:1807.07247v3
8. Guan, Qingji, and Yaping Huang. Multi-Label Chest X-Ray Image Classification via Category-Wise Residual Attention Learning. Pattern Recognition Letters, vol. 130, 2020, pp. 259?266., doi:10.1016/j.patrec.2018.10.027.
9. Rubin, Jonathan, et al. Large Scale Automated Reading of Frontal and Lateral Chest X-Rays using Dual Convolutional Neural Networks, 2018, arXiv:1804.07839
10. Yasaka K, Abe O. Deep learning and artificial intelligence in radiology: Current applications and future directions. PLOS Medicine 2018;15. doi:10.1371/journal.pmed.1002707
11. Dai JJ, Li Z, Wang J, et al. BigDL. Proceedings of the ACM Symposium on Cloud Computing - SoCC 19 Published Online First: 2019. doi:10.1145/3357223.3362707
12. Huang G, Liu Z, Maaten LVD, et al. Densely Connected Convolutional Networks. 2017 IEEE Conference on Computer Vision and Pattern Recognition (CVPR) Published Online First: 2017. doi:10.1109/cvpr.2017.243
13. He K, Zhang X, Ren S, et al. Deep Residual Learning for Image Recognition. 2016 IEEE Conference on Computer Vision and Pattern Recognition (CVPR) Published Online First: 2016. doi:10.1109/cvpr.2016.90